energies

MDPI

Article

Toward a Sustainable Indoor Environment: Coupling Geothermal Cooling with Water Recovery Through EAHX Systems

Cristina Baglivo [1], Alessandro Buscemi [2], Michele Spagnolo [1], Marina Bonomolo [2], Valerio Lo Brano [2,*] and Paolo Maria Congedo [1]

[1] Department of Engineering for Innovation, University of Salento, 73100 Lecce, Italy; cristina.baglivo@unisalento.it (C.B.); michele.spagnolo@unisalento.it (M.S.); paolo.congedo@unisalento.it (P.M.C.)
[2] Department of Engineering, University of Palermo, 90128 Palermo, Italy; alessandro.buscemi@unipa.it (A.B.); marina.bonomolo@unipa.it (M.B.)
* Correspondence: valerio.lobrano@unipa.it

Abstract: This study presents a preliminary analysis of an innovative system that combines indoor air conditioning with water recovery and storage. The device integrates Peltier cells with a horizontal Earth-to-Air Heat Exchanger (EAHX), exploiting the ground stable temperature to enhance cooling and promote condensation. Warm, humid air is pre-cooled via the geothermal pipe, then split by a fan into two streams: one passes over the cold side of the Peltier cells for cooling and dehumidification, while the other flows over the hot side and heats up. The two airstreams are then mixed in a water storage tank, which also serves as a thermal mixing chamber to regulate the final air temperature. The analysis investigates the influence of soil thermal conditions on condensation within the horizontal pipe and the resulting cooling effect in indoor spaces. A hybrid simulation approach was adopted, coupling a 3D model implemented in COMSOL Multiphysics® with a 1D analytical model. Boundary conditions and meteorological data were based on the Typical Meteorological Year (TMY) for Palermo. Two scenarios were considered. In Case A, during the hours when air conditioning is not operating (between 11 p.m. and 9 a.m.), air is circulated in the exchanger to pre-cool the ground and the air leaving the exchanger is rejected into the environment. In Case B, the no air is not circulated in the heat exchanger during non-conditioning periods. Results from the June–August period show that the EAHXs reduced the average outdoor air temperature from 27.81 °C to 25.45 °C, with relative humidity rising from 58.2% to 66.66%, while maintaining nearly constant specific humidity. The system exchanged average powers of 102 W (Case A) and 96 W (Case B), corresponding to energy removals of 225 kWh and 212 kWh, respectively. Case A, which included nighttime soil pre-cooling, showed a 6% increase in efficiency. Condensation water production values range from around 0.005 g/s with one Peltier cell to almost 0.5 g/s with seven Peltier cells. As the number of Peltier cells increases, the cooling effect becomes more pronounced, reducing the output temperature considerably. This solution is scalable and well-suited for implementation in developing countries, where it can be efficiently powered by stand-alone photovoltaic systems.

Keywords: earth-to-air heat exchanger system (EAHXs); peltier cells; geothermal cooling; finite element method (FEM)

Academic Editor: Javier F. Urchueguía

Received: 31 March 2025
Revised: 19 April 2025
Accepted: 24 April 2025
Published: 30 April 2025

Citation: Baglivo, C.; Buscemi, A.; Spagnolo, M.; Bonomolo, M.; Lo Brano, V.; Congedo, P.M. Toward a Sustainable Indoor Environment: Coupling Geothermal Cooling with Water Recovery Through EAHX Systems. *Energies* **2025**, *18*, 2297. https://doi.org/10.3390/en18092297

1. Introduction

One effective approach to addressing the challenges of the energy crisis in developing countries is adopting geothermal resources. Surface geothermal energy is an optimal option because it is widely accessible, reliable, and environmentally friendly [1].

The earth air heat exchanger system (EAHXs) includes horizontal underground pipes, generally placed close to buildings. These systems exploit the subterranean heat to treat the air passing through buried pipes. Geothermal systems can reduce energy consumption and consequently improve the energy efficiency of buildings thanks to the use of the ground as an easily accessible source or reservoir of heat [2]. This renewable and sustainable form of energy is constantly provided by nature and can be utilized year-round [3]. The EAHXs utilizes the ground's stable temperature, a few meters under the surface allowing the exchange of heat with the air [4]. Unlike the seasonal variations in external air temperature, the ground temperature remains relatively constant, being cooler than the air during the summer season and warmer during the winter season [5–7]. With its straightforward design and minimal upfront expenses, EAHXs provides benefits like energy efficiency and excellent performance year-round [8], reducing reliance on conventional air conditioning systems and advocating energy conservation and sustainable building practices. In several studies, the GSHP models do not consider certain factors, e.g., buried piping, soil, and actual operating conditions.

Nevertheless, the performance of these systems depends on several factors such as backfill material characteristics, U-tube pipe properties, borehole depth, soil thermal features, heat carrier fluid type and fluid velocity, and spacing. It also studied the influence of the systems on heat transfer efficiency and reported solutions for improving performance [9]. Luo et al. [10] studied the performance of a "slinky" ground heat exchanger. This latter is based on a validated transient model to analyze the effect of the different conditions (e.g., daily operation hours, installation depths, soil characteristics, and trench separations).

In Ref. [11] the EAHXs is evaluated in various climates and soils; in Refs. [12,13] authors tested these systems in extremely hot climates. Hollmuller et al. [14] analyzed the underground pipe system in central European climates. The study in Ref. [15] analyzed the potential impact of a dynamic thermal environment characterized by significant seasonal fluctuations in outdoor climatic conditions and large fluctuations in ground surface temperatures on the practical implementation of EAHXs. The research then investigated an EAHXs in cold-arid areas of northwestern China, revealing a robust heat exchange capacity in both winter and summer and that the outlet temperature ranges more uniformly during winter. The borehole heat exchanger (BHE) has a crucial role in the system because its performance widely influences the cost of the whole system [16]. Its behavior depends on air temperature, seepage flow rate, ground temperature gradient, and injection flow rate, but the literature lacks field test verification.

Many studies in the literature have investigated how airflow parameters, pipe characteristics, and configurations influence the performance of EAHXs [17–19]. Furthermore, at equal pipe lengths, the choice between steel or polyvinyl chloride (PVC) material does not notably impact performance, indicating that the high thermal conductivity of steel pipes does not notably enhance overall heat transfer [20]. Alqawasmeh et al. [21] applied a 3D finite element numerical method to study vertical energy piles with different diameters equipped with parallelly connected U-tube and W-tube GHEs. In their study, authors considered important aspects such as the conductivities of ground and concrete fluid flow rate, GHE pipe diameter, pile spacing, and pile length. Zhou et al. [22] developed a 3D finite element model, but for a horizontal pipe by using COMSOL Multiphysics 3.3 and validated it by using measurements in a rural industry in Australia. They considered

different configurations, thermal conductivity, and different trench separations (from 1.2 to 3.5 m).

The combined use of solar and geothermal systems for space heating and cooling is a very effective strategy to ensure year-round thermal comfort and maximize energy efficiency [23]. Ghiasi et al. [24] analyzed a system that integrated photovoltaic system of an unglazed building, a horizontal ground heat exchanger, and a heat pump system from a water source for a greenhouse agriculture highlighting potential cost savings and system efficiencies.

Additionally in Ref. [25] authors investigated an innovative offset pipe energy foundation pile functioning as a ground heat exchanger integrated with solar photovoltaic/thermal collectors. Long-term performance results indicate that incorporating solar thermal energy mitigates ground thermal imbalance, improving from −0.27 K/year to a nearly balanced state (~0.01 K/year). Shahsavar et al. [26] assessed the feasibility of an integrated system combining an EAHXs with a photovoltaic/thermal unit enhanced by phase change material to fulfill a building's heating, cooling, and electricity demands. Bhutta et al. [27] demonstrated that computational fluid dynamics (CFD) serves as a reliable method for the precise analysis of various heat exchanger types. The study [28] employed CFD Fluent to examine heat exchange within EAHXs, revealing that key parameters influencing heat transfer performance include the velocity of the fluid inside the tubes and the burial depth of the heat exchangers. In this light, it is fundamental to develop and adopt the optimized methodology that analyze the behavior of the fluids in specific conditions. The studies conducted in [29] focused on a simplified mathematical model of heat transfer to predict long-term changes in the temperature of the ground in which a horizontal ground heat exchanger has been installed. Furthermore, of fundamental importance is that the integration of ground-to-air heat exchangers with solar greenhouses can be a sustainable solution for maintaining optimal growing conditions in the face of climate change, allowing for water-saving potential [30].

Aim of the Work

This study presents a preliminary analysis for developing a low-energy indoor air conditioning and water recovery system. The proposed device integrates Peltier cells with a horizontal EAHXs, utilizing stable ground temperatures to enhance cooling and promote condensation. Warm, humid air is first pre-cooled via the geothermal pipe, then divided by a fan into two streams: one passes over the cold side of the Peltier cells for cooling and dehumidification, while the other flows over the hot side and heats up. Both streams are then mixed in a water storage tank, which also acts as a thermal mixing chamber to regulate the outlet air temperature. The system enables water collection through condensation and offers a simple alternative to traditional heat pumps and air handling units.

The concept of extracting water from air is not new, but it is often associated with costly and complex technologies. In contrast, this system aims to offer a simple, low-cost, and eco-friendly solution that can be built locally using readily available materials. The system is designed for on-site construction, utilizing components such as plastic tubing for geothermal pipes and Peltier cells repurposed from old computers or refrigerators. This accessible approach makes it especially suitable for developing regions where access to clean water is limited, offering significant humanitarian benefits. What makes this idea particularly innovative is its creative adaptation of technologies typically used for cooling electronic devices, applying them to geothermal systems to enhance and expand their capabilities.

2. Methodology

This study should be regarded as a preliminary investigation to evaluate the energy analysis of an air soil exchanger. The methodology proposed is based on a Finite Element Method (FEM). The solution was implemented by combining a 3D model, developed in COMSOL Multiphysics® 3.3, with a 1D model. The first one was developed to study thermal conduction in the soil. The numerical model was calibrated using extensive experimental data from Palermo, including soil thermal profiles and boundary conditions measured over more than a year. These latter were modeled by using an analytical solution and measurements taken from a real case study (described in detail in Section 3). The second model was used to analyze the moist-air cooling phenomena. In this case, the Typical Meteorological Year (TMY) of Palermo was used. Figure 1 shows the flux diagram of the methodology applied.

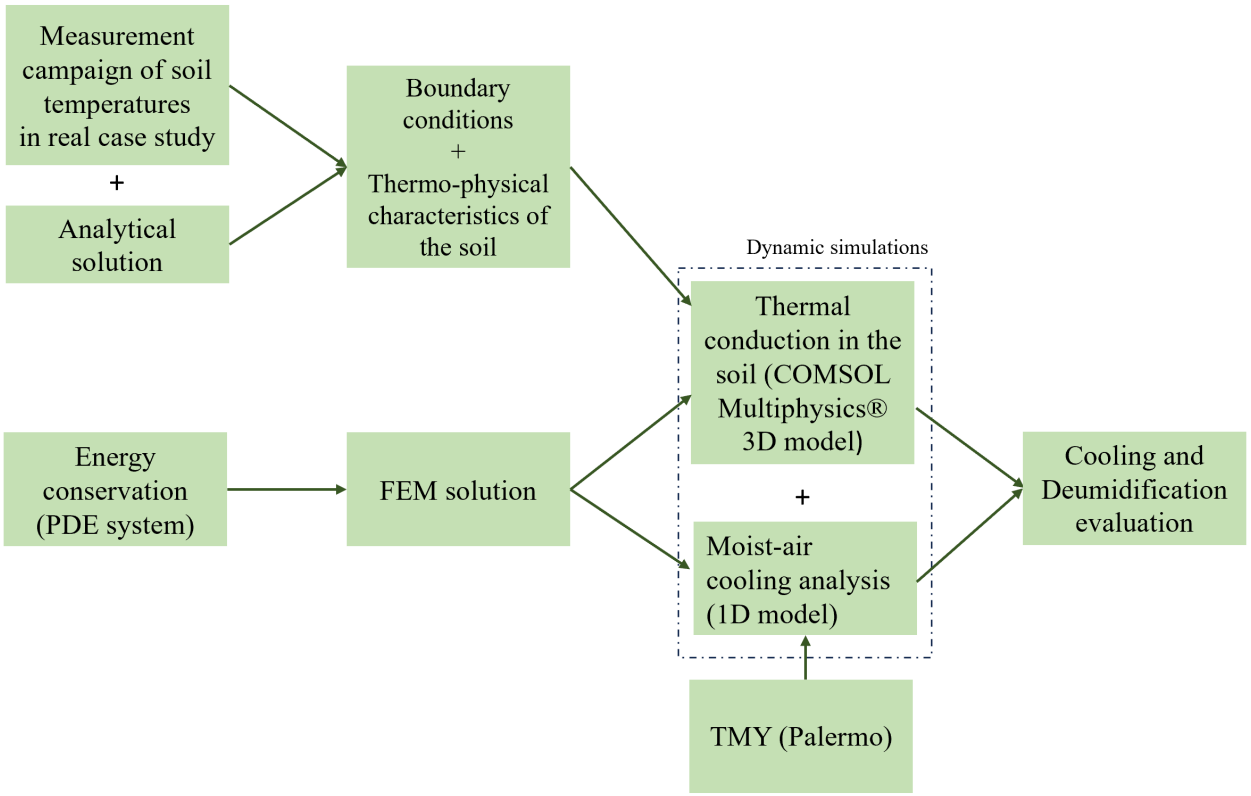

Figure 1. A concept graph of the methodology applied.

Subsequently, the output data from the geothermal probe are used to model the last section of the probe within which the Peltier cells are placed. Based on the temperature and relative humidity values, thermodynamic properties are derived, including the humidity ratio, dew point temperature, and specific enthalpy. In particular, by knowing the cooling power of the Peltier cells and the dry air flow rate, the enthalpy reduction due to heat extraction is quantified. Moreover, the enthalpy of the dry air stream at saturation is evaluated. By comparing this value with the enthalpy after the cooling phase, it is possible to determine whether condensation occurs within the system.

2.1. Formulation of the Equations of the New Finite Element Model

The new multi-physical model of the EAHXs allows dynamic simulation of temperature and relative humidity variations in humid air along the exchanger. This model is based on the energy balance of the soil around the heat exchanger and that of the heat transfer fluid, which in this case is humid air as described below.

The energy balance equations of the three-dimensional soil volume can be represented by the following Partial Differential Equation (PDE) [31]:

$$C_s \cdot \frac{dT_s}{dt} = \nabla \cdot (\lambda_s \cdot \overline{\nabla} T_s) \quad (1)$$

where C_s is the volumetric heat capacity of the soils [J·m^{-3}·K^{-1}], T_s the temperature of the soil [K], t the time [s], and λ_s the thermal conductivity of the soil [W·m^{-1}·K^{-1}]. On the upper boundary of the domain (interface between the soil and the atmosphere), a Dirichlet condition characterized by a periodic change in the superficial temperature T_{sup} [K] over time is assumed [30]:

$$T_{sup}(d) = T_0 + B \cdot \sin[\omega \cdot (d - d^*)] \quad (2)$$

where d is the time [day], T_0 is the annual average value of T_{sup} [K], B the amplitude of the sinusoid [°C]; ω is the pulsation [day^{-1}] and, d^* a time-lag [day] constant. The pulsation, in particular, can be calculated as $\omega = 2 \cdot \pi / \tau$ where τ [day] is the period that is fixed equal to τ = 365 day. Moreover, considering that for a soil domain represented by an infinitely extended half-space subject to a surface boundary temperature condition of periodic type, such as that described by Equation (2), the temperature variation in time and space can be described by the following analytical solution [30]:

$$T_s(z;d) = T_0 + B \cdot e^{-\gamma \cdot z} \cdot \sin[\omega \cdot (d - d^*) - \gamma \cdot z], \ \forall z \in I \subset \mathbb{R} \quad (3)$$

where z is the vertical coordinate representing the depth in the soil relative to the ground plane [m] and, γ a damping constant [m^{-1}] that can be calculated as [30]:

$$\gamma = \sqrt{\omega / (2 \cdot \alpha_s)} \quad (4)$$

where α_s is the thermal diffusivity of the soil [m^2·day^{-1}]. Following this approach, Equation (3) was used in the proposed model to define the undisturbed initial soil temperature distribution $T_s(z;0)$ at all points in the domain (at intial time for each value of z) and the changes in $T_s(z_{inf};d)$ over time in the lower boundary of the domain (at $z = z_{inf}$). In the latter case, the value of z_{inf} [m] should be chosen high enough to consider this lower boundary undisturbed by the heat fluxes exchanged between the EAHXs and the ground.

The energy balance of the air circulating within the EAHXs can be described by means of the following mono-dimensional advective-convective PDE [31]:

$$\rho_a \cdot c_{pa} \cdot A_{pi} \cdot \frac{\delta T_a}{\delta t} + \frac{\delta}{\delta x} \left(-\lambda_a \cdot \frac{\delta T_a}{\delta x} \right) \cdot A_{pi} = -\dot{q}_{as} - \dot{m}_a \cdot c_{pa} \cdot \frac{\delta T_a}{\delta x} \quad (5)$$

where x is the coordinate describing the linear distance from the inlet of the pipe [m], ρ_a the fluid density [kg·s^{-1}], c_{pa} the specific heat of the fluid [J·kg^{-1}·K^{-1}], A_{pi} the internal cross-sectional area of the pipe [m^2], T_a the cross-sectional average air temperature at x [K], λ_a the thermal conductivity of the air [W·m^{-1}·K^{-1}], $\dot{q}_{as}$ the thermal power exchanged per unit length of pipe [W·m^{-1}] and, $\dot{m}_a$ the mass flow rate of the fluid circulating in the EAHXs [kg·s^{-1}]. In the above expression, the heat flux $\dot{q}_{as}$, assumed positive if released by the air, can be calculated at each x along the pipe through the following expression [30]:

$$\dot{q}_{as}(x) = \frac{T_a(x) - T_{p,e}(x)}{R_{ap} + R_{ps}} \quad (6)$$

in which $T_{p,e}$ is the outer pipe wall temperature at x [K], R_{ap} is the fluid-soil equivalent thermal resistance [K·m·W^{-1}], and R_{ps} the conductive thermal resistance of the pipe material [K·m·W^{-1}]. The first term, for a circular pipe, can be expressed as [30]:

$$R_{ap} = \frac{1}{\pi \cdot D_{p,i} \cdot h_{conv}} \tag{7}$$

where $D_{p,i}$ is the inner diameter of the pipe [m] and h_{conv} is the convective heat transfer coefficient [W·m^{-2}·K^{-1}]. This coefficient can, in turn, be calculated from the following relationship [30]:

$$h_{conv} = \frac{\lambda_a \cdot Nu}{D_{p,i}} \tag{8}$$

where Nu is the Nusselt number which, in the case of purely turbulent flow (which occurs for Reynold numbers above Re = 4000) can be expressed by the following empirical function [32]:

$$Nu = \frac{\frac{\xi}{8} \cdot (Re - 1000) \cdot Pr}{1 + 12.7 \cdot \sqrt{\frac{\xi}{8}} \cdot (Pr^{\frac{2}{3}} - 1)} \tag{9}$$

where ξ is the friction factor and Pr the Prandtl number. The term conductive resistance, which appears in Equation (3), can instead be expressed as [30]:

$$R_p = \frac{\ln\left(\frac{D_{p,o}}{D_{p,i}}\right)}{2 \cdot \pi \cdot \lambda_p} \tag{10}$$

where $D_{p,o}$ is the outer diameter of the pipe [m] and λ_p the thermal conductivity of the pipe material [W·m^{-1}·K^{-1}].

It is important to emphasize that the coupling between Equations (1) and (5) in the model is achieved through a specific mixed boundary condition imposed at the outer surface of the heat exchanger tube, which interfaces with the 3D solid domain representing the soil surrounding the EAHXs. The implementation of this condition is carried out by introducing an additional weak term—formulated using COMSOL's custom weak form interface—into the finite element model. This approach enables the simultaneous enforcement of a Neumann boundary condition ($\dot{q}_{as}$) and a Dirichlet boundary condition ($T_{p,e}$) at each spatial location x along the surface of a common boundary. Both quantities, which are treated as space- and time-dependent unknowns, are resolved through a dedicated use of COMSOL's general extrusion operators.

With regard to all thermophysical properties of air, it is assumed that they are equal to those of dry air because below about 40 °C these properties can be considered equivalent to those of moist air for any relative humidity RH [%] [33]. Accordingly, the thermophysical properties employed in Equations (5), (8) and (9) were assumed to depend solely on temperature T_a, which, as previously discussed, varies along the length of the pipe as a result of heat exchange with the surrounding soil.

Furthermore, although the assumptions underlying the proposed model allow for the simulation of cooling processes without dehumidification (i.e., assuming constant absolute humidity of the air), they still enable the identification of potential incipient water vapor condensation conditions on the inner surface of the EAHXs. For this purpose, the dew-point temperature T_{dp} [K] can be calculated from the partial vapor pressure p_v [N·m^{-2}], which is considered constant throughout x, through the following relationship [34]:

$$p_v = p_{vs}(T_{a,in}) \cdot (RH_{in}/100) \tag{11}$$

where p_{vs} is saturation vapor pressure of water [N·m^{-2}], $T_{a,in}$ the air temperature at the entrance of the EAHXs (x = 0) [K] and, RH_{in} the air relative humidity at the same position [%]. The T_{dp} is then compared, for each value of x, with the EAHXs internal wall temperature $T_{p,i}$ [K] which can be derived from the following relationship:

$$T_{p,i}(x) = T_a(x) - \dot{q}_{as}(x) \cdot R_{ap} \quad (12)$$

where both $T_a(x)$ and $\dot{q}_{as}(x)$ are calculated by the finite element (FE) model at each time step. Therefore, whenever T_{dp} is equal to or greater than $T_{p,i}$ at some x position along the exchanger the conditions of possible water condensation can be identified. In any case, the model allows the relative humidity conditions of the air flowing through the duct (and thus also those at the outlet) to be evaluated through the use of the following relationship [34]:

$$RH(x) = \frac{p_v}{p_{vs}[T_a(x)]} \quad (13)$$

where p_v is calculated using Equation (11) and $T_a(x)$ comes from the numerical solution of the boundary value problem. In order to facilitate comprehension of the material presented in this section, a schematic flowchart of the EAHX physical–mathematical model has been provided in Figure 2.

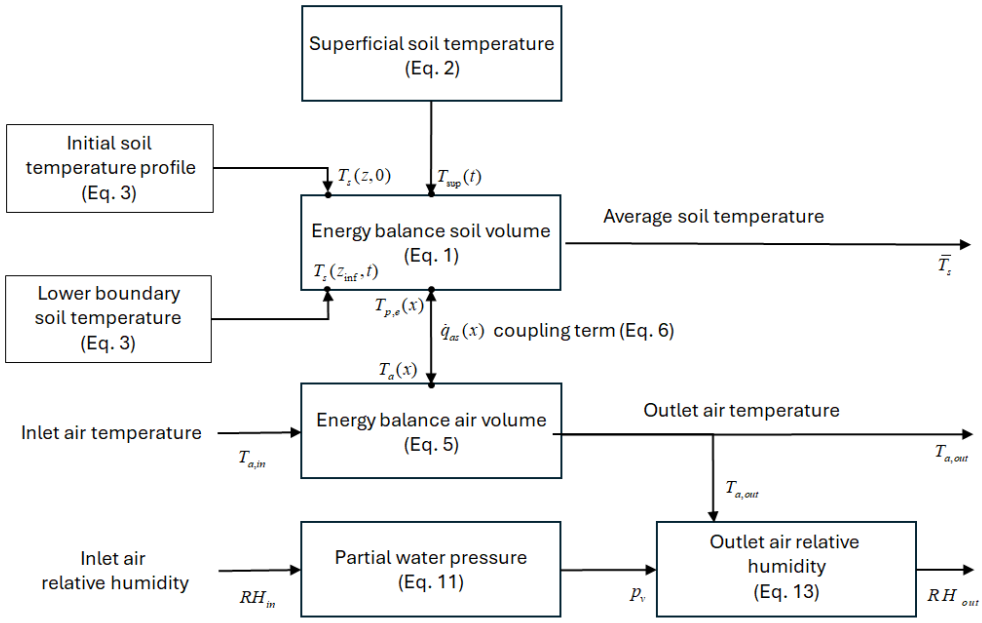

Figure 2. Flowchart of the EAHX physical mathematical model.

2.2. The Proposed System

To enhance the thermal effect achieved through geothermal exchange, the system integrates thermoelectric Peltier cells. These devices amplify the heat transfer process started in the geothermal probe. As outdoor air enters the probe, it undergoes preliminary thermal conditioning, primarily pre-cooling. When the air temperature falls below the dew point, moisture begins to condense inside the probe.

At the probe outlet, a longitudinal partition splits the pipe into two semi-cylindrical channels (Figure 3), with Peltier cells installed along the dividing surface. These cells are sequentially activated to gradually increase the system's thermal output. The airflow is divided accordingly: one stream travels along the cold side of the Peltier cells for further cooling and dehumidification (represented by blue arrows), while the other passes over the hot side for heating (red arrows).

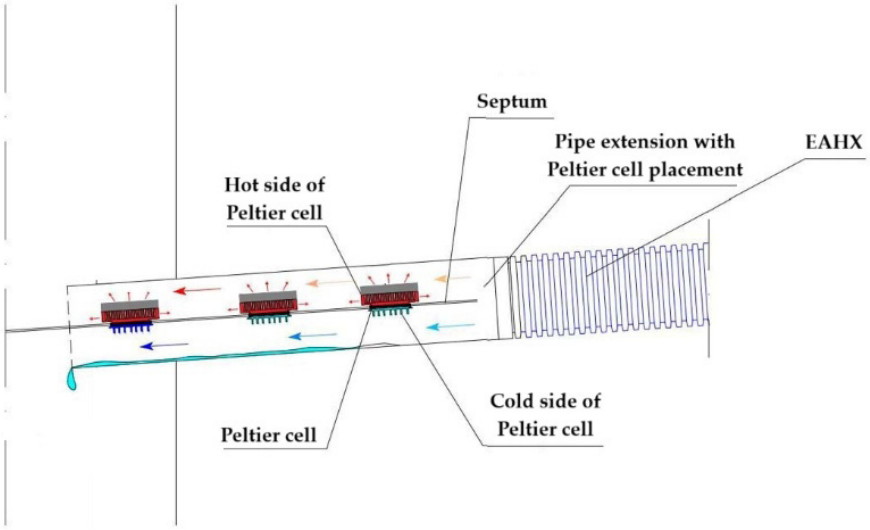

Figure 3. Last section of the geothermal pipe with Peltier cells.

Condensed water from the cold side flows downward by gravity into a collection tank, which also functions as a mixing chamber. Depending on the desired indoor conditions, the two airstreams can either be delivered separately or mixed adiabatically. For maximum cooling efficiency, only the cold air is supplied to the room; when heating is needed, the cold and warm flows are recombined before distribution. A full description of the system can be found in the study [35].

The entire system can operate autonomously, with fans and Peltier modules powered by renewable energy sources such as photovoltaic panels and micro wind turbines.

3. Case Study and Calibration of the Model

The approach outlined in the previous section was used to define a FE model of a single EAHXs unit consisting of a cross-linked polyethylene (PE) pipe (λ_p = 0.42 W·m^{-1}·K^{-1}), installed at a depth of 2.5 m. The three-dimensional computational FE domain, illustrated in Figure 4, is a quadrangular prism measuring 24 m in length, 10 m in width, and 10 m in depth (z_{inf}). Within the soil domain, a semi-cylindrical void with a diameter of $D_{p,e}$ = 200 mm is included to represent the space occupied by the heat exchanger pipe, whose internal diameter is set to $D_{p,i}$ = 186.4 mm. The dimensions of the heat exchanger tube (both diameters and length) correspond to commercially available products.

In addition, a sinusoidal boundary condition for the upper surface based on daily averaged on-site soil temperature measurements wase used to capture local ground conditions. While this approach does not fully reproduce diurnal temperature swings, the influence of these fluctuations is negligible at the pipe burial depth due to significant thermal damping. To implement such conditions, it was assumed that the cooling system at the campus of the University of Palermo where undisturbed subsurface thermal profiles and thermophysical properties of different soil layers were recently studied through experimental and numerical analyses was used [30].

This made it possible to calibrate the new FE model with realistic parameters. Specifically, the undisturbed thermal profiles were obtained through an experimental campaign in which soil temperatures were measured by means of five different thermal sensors (PT100) that were installed at different depths (A z = 0.15 m, B z = 0.27 m, C z = 1.27 m., D z = 2.27 m., E z = 4.27 m, F z = 7.27 m) along a Borehole Heat Exchanger (BHE).

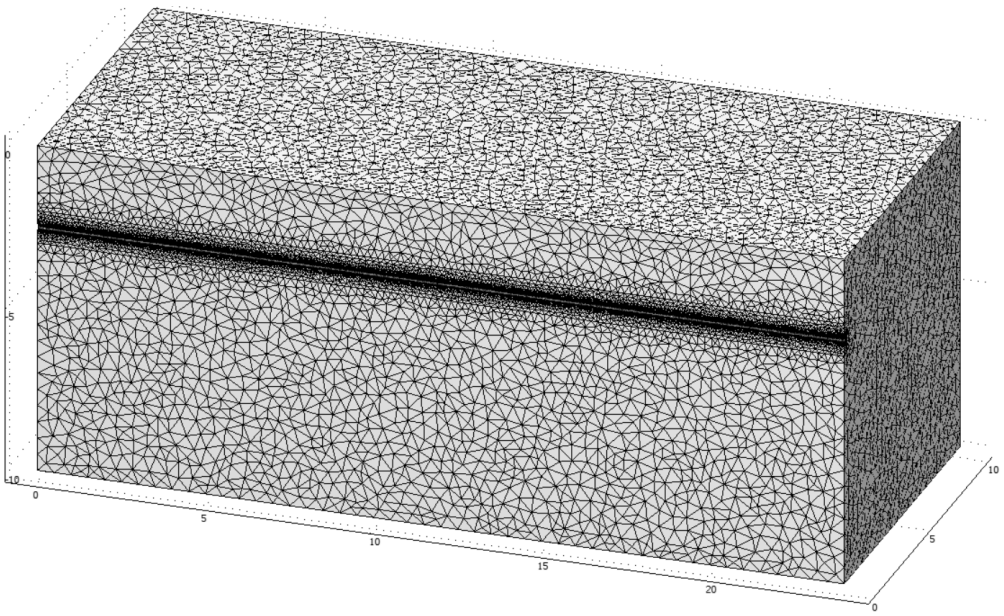

Figure 4. Soil domine of the three-dimensional FE model of the EAHE.

These measurements, taken with a timestep of 10′, allowed reconstruction of the thermal profiles described in Figure 5 (adapted from [30]). The measured data, exhibiting a sinusoidal-type trend, shows two consecutive thermal peaks due to the execution of two Thermal Response Tests (TRTs) carried out on the BHE at the beginning of the experimental campaign. The same data show that in the summer period, the cooling effect due to groundwater is close to that depth. Moreover, data recorded from the deepest sensor (F) show that in the summer period, the cooling effect due to groundwater is close to that depth.

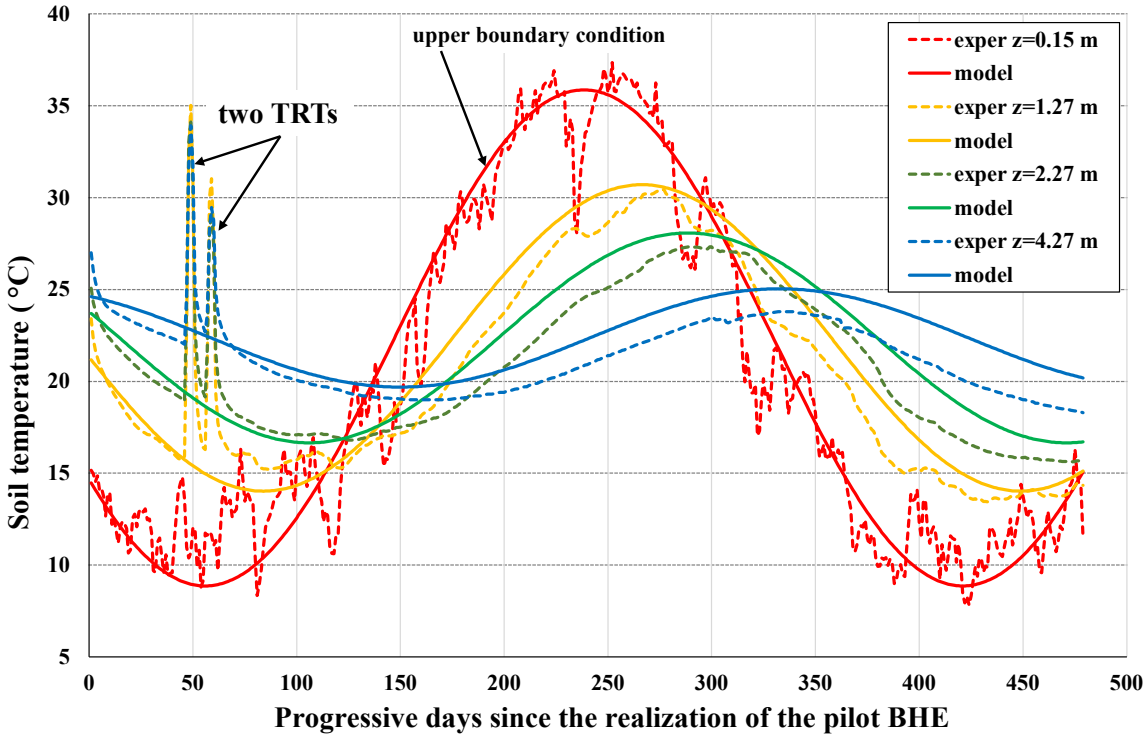

Figure 5. Comparison of changes in daily average subsoil temperatures in Palermo, measured (dashed lines) and obtained from the analytical solution (solid lines), at varying depths. Adapted from Ref. [30].

The shallower sensor temperature data, represented by a red curve in Figure 5, was a fit with the Equation (2). Based on the interpolation, carried out with the least squares method, the parameters summarized in Table 1 were obtained. Moreover, the analytical solution described by Equations (3) and (4) were used to model the daily temperature variations measured at different depths z of the remaining five thermal sensors.

Table 1. Parameters of the undisturbed thermal profile of the Palermo subsurface.

T_0 [°C]	B [°C]	d^* [day]	τ [day]	ω [1/day]	γ [1/m]
22.36	13.50	147.19	365	0.017214	0.379117

For this purpose, the least-squares method was employed to minimize the quadratic differences between the measured and modeled temperature values in order to estimate the soil thermal diffusivity α_s value. As a result of these computations, a value of α_s = 0.06 m^2/day was derived, which inserted into the analytical expression allows the thermal profiles to be derived over time as depth changes as shown in Figure 5.

In addition, numerical experimental analysis performed on the same soils through TRTs on the pilot BHE yielded a value of the average thermal conductivity of the soils equal to λ_s = 1.68 W/(m K) [30]. Finally, from the α_s and λ_s values obtained, it was possible to deduce an average volumetric heat capacity of the soil of C_s = 2.51·10^6 J/(m^3·K).

Numerical analyses were conducted considering the period comprised between 1 June and 7 September of the TMY assuming that the building's air-conditioning system operated continuously between 10:00 am and 10:00 pm. The flow rate of moist air considered in the duct was assumed to be $\dot{m}_a$ = 0.077 kg/s (which corresponds, at an average dry air temperature of 25 °C to a Reynolds number of about 29,680), and the time series of $T_{a,in}$ and RH_{in} values were generated from a TMY generated for the Palermo area.

Finally, two scenarios were considered:

- Case A: during the hours when air conditioning is not operating (between 11 p.m. and 9 a.m.), air is circulated in the exchanger to pre-cool the ground. In this phase, the air leaving the exchanger is rejected into the environment. For the purpose of these analyses, it was assumed that the nightly recirculation of pre-cooled soil air is only active when the outside air temperature is lower than the internal pipe temperatures at the duct inlet.
- Case B: no air is circulated in the heat exchanger during non-conditioning periods.

4. Results and Discussion

Figure 6 shows results of the numerical simulations in the form of contour plots of the relative changes in soil temperatures around the EAHXs (compared with undisturbed soil), derived from Equations (3) and (4). From this figure, one can infer which region, in terms of volume, is most affected by thermal gradients.

A more detailed analysis of the first three months of operation (1 June and 7 September of a TMY) is presented below. During these months, the EAHXs is able to cool humid outside air by reducing its temperature and relative humidity, on average, from $T_{a,in}$ = 28 °C and RH_{in} = 58% to $T_{a,out}$ = 25.5 °C and RH_{out} = 66.40%, respectively.

Thus, the system can cool the outside ai by about 2.5 °C while keeping the specific humidity of the incoming air nearly constant for most of the analyzed period. However, Figure 7 (which reports the air temperature values during one week in June) shows that the temperature reduction predicted by the simulations can be as high as 7.43 °C. In that same week, the EAHXs reaches its maximum peak cooling output of about 576 W, corresponding to approximately 4 W/m of cooling per unit length of the thermal exchanger.

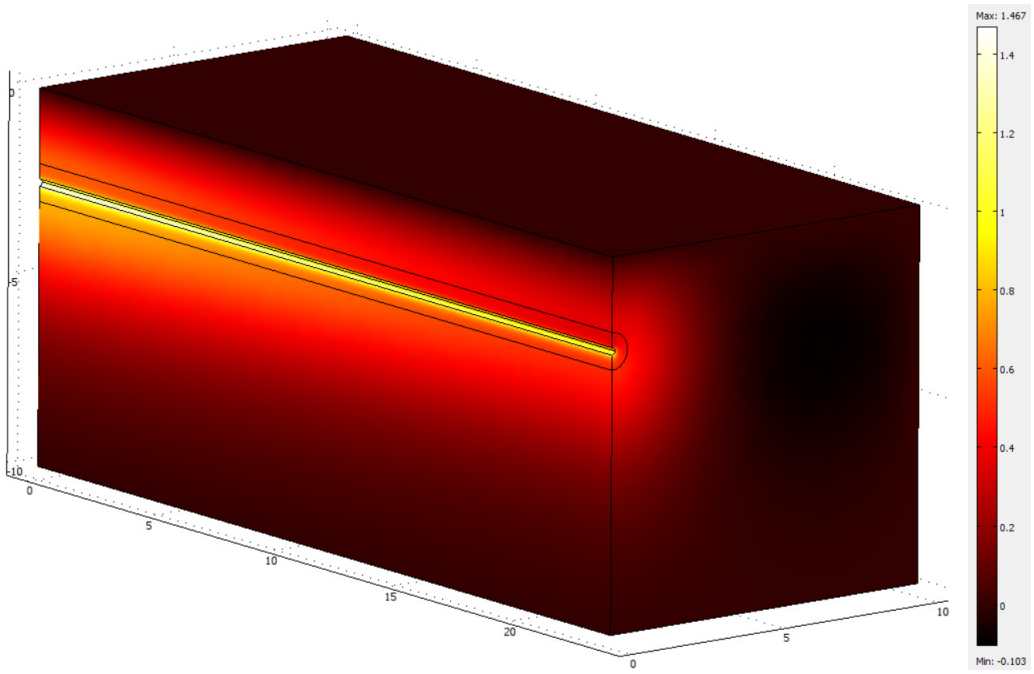

Figure 6. Contour plot showing the increases, compared to undisturbed values, in soil temperature around the EAHX (FE simulations).

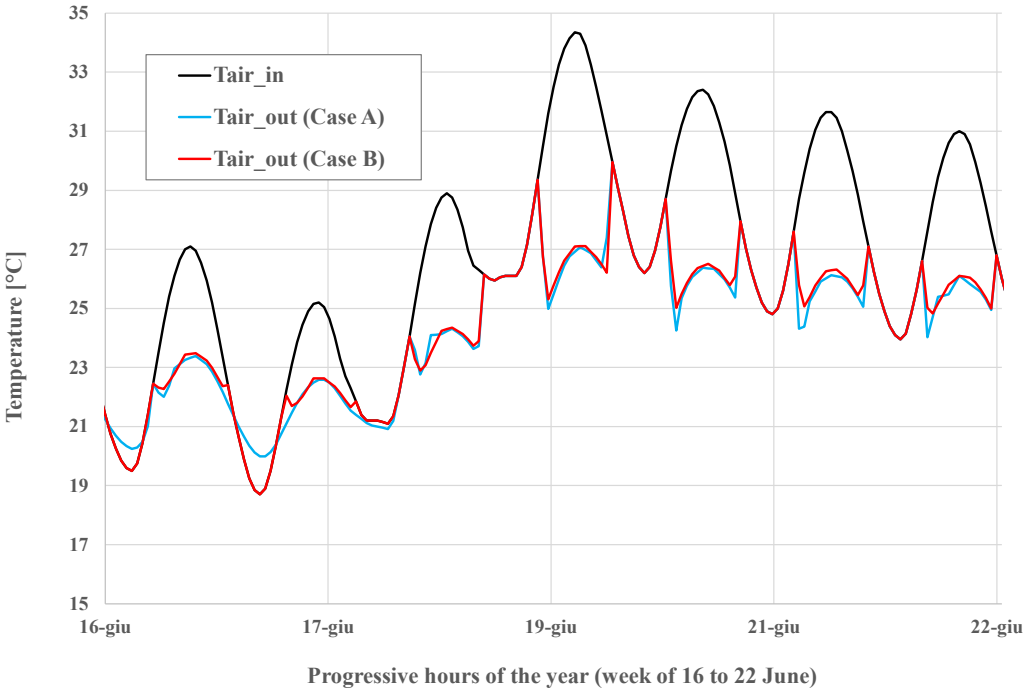

Figure 7. Variations in air temperature at the inlet and outlet of the heat exchanger (for Case A and Case B, respectively) in a week of June (FE simulation).

The power exchange calculations for the two scenarios (see Figure 8) show that, over the analyzed period, the average powers exchanged in Case A and Case B are 187.89 W and192.85 W, respectively. These values correspond to total heat energy removed from the air of 239.37 kWh and 222.55 kWh, respectively. These preliminary results indicate that pre-cooling the soil at night (Case A) can increase the EAHXs's efficiency by about 7.56% compared with Case B. Figure 8 also shows the periods when thermal power was extracted from the soil (negative values) in the nighttime pre-cooling phases. Due to this

mode of operation, the heat powers exchanged in Case A are slightly higher, especially in the second half of the cooling period.

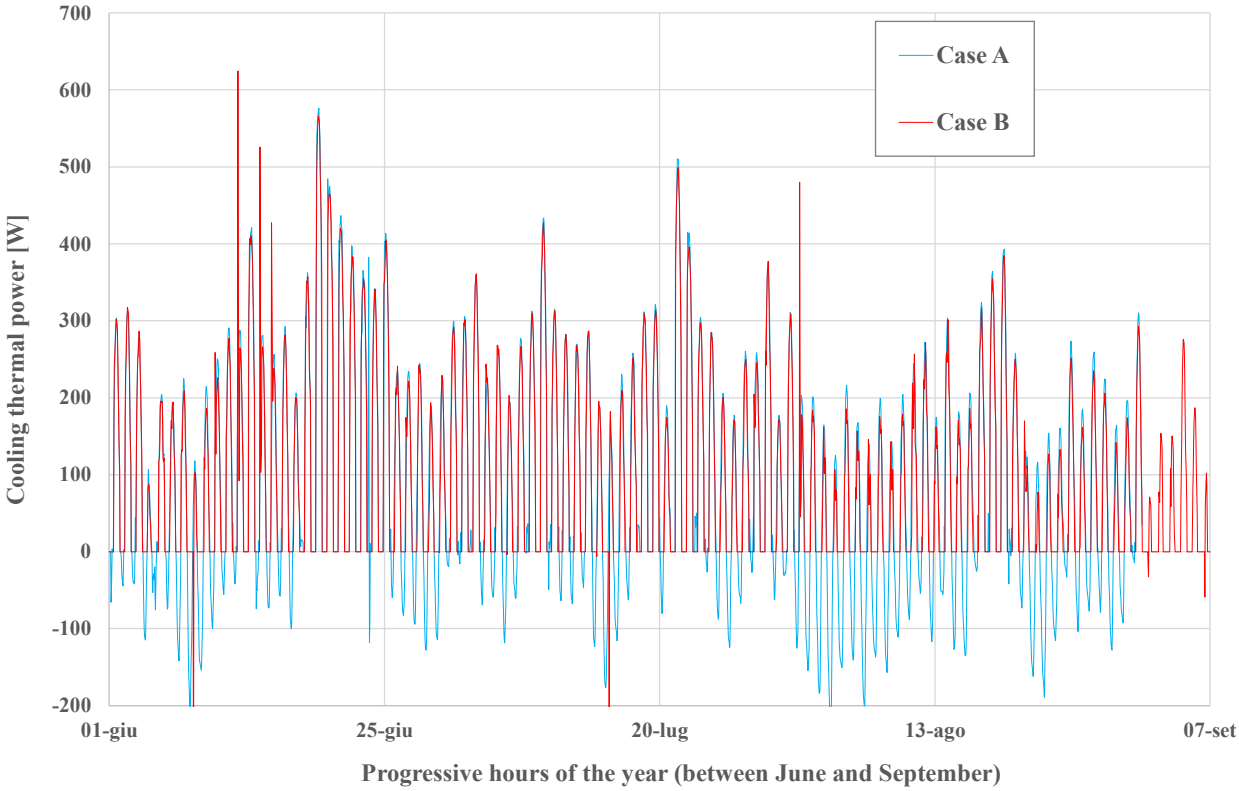

Figure 8. Hourly variations in heat exchanger cooling capacities for the two cases analyzed in the months between June and August (FE simulations).

To assess the potential for water condensation on the inner surface of the tube, the temperatures of the inner wall at the inlet and outlet sections were compared with the calculated dew point values (see Figure 9). The results show that condensation conditions occurred only sporadically (for about 10 h out of a total of 1196 h of operation). This suggests that the numerical model presented here requires further development to simulate the heat transfer processes that occur under water vapor condensation.

Figure 9 also shows a gradual increase in the inner wall temperature of the tube over the operational period. To better investigate this aspect, the temperature difference relative to a scenario with no heat exchange was calculated for a cylindrical soil volume (radius = 1 m) around the exchanger tube.

The results of the latter analyses are illustrated in Figure 10, which shows, for the period under consideration, the changes in mean soil temperature from undisturbed values for the two cases analyzed. On average, the temperature increments (soil thermal drift) are 1.37 °C and 1.66 °C, respectively, for Case A and Case B. Thus, the pre-cooling method succeeds, albeit marginally, in reducing temperature increases, especially after the second half of August as is evident from Figure 10. These findings highlight the need for additional multi-year dynamic simulations to fully evaluate the long-term thermal response of the exchanger–soil system.

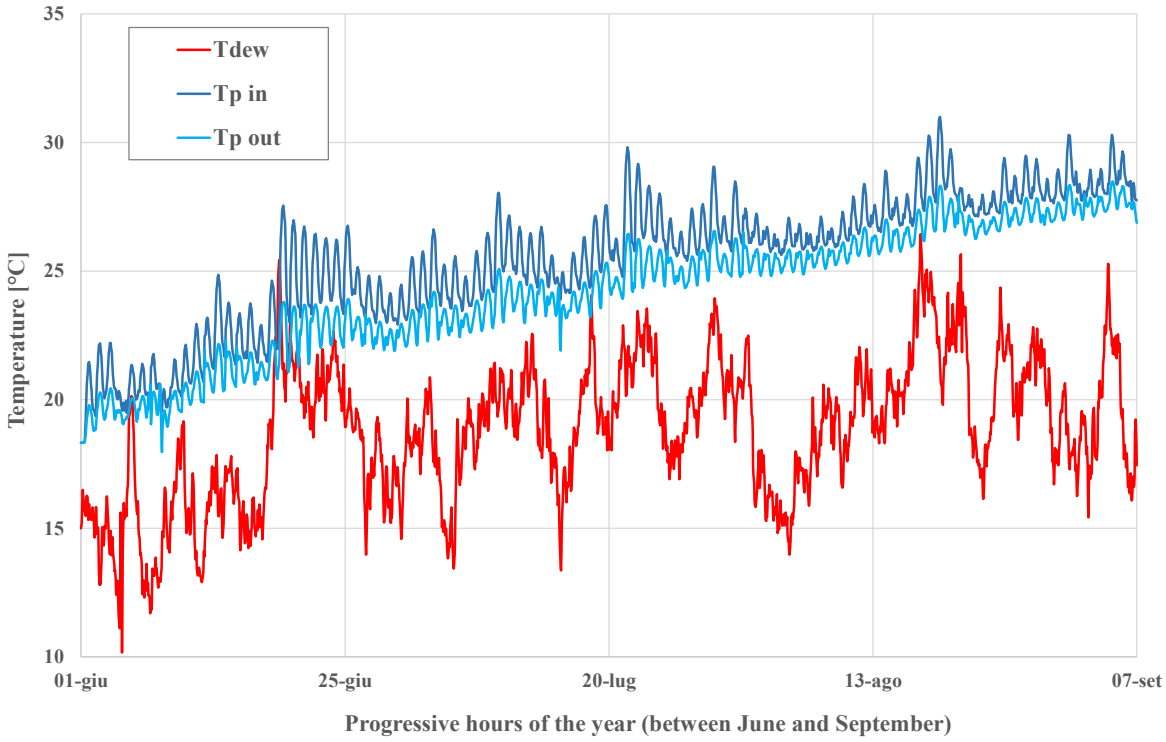

Figure 9. Comparison of the simulated variations in the internal pipe wall temperatures (inlet and outlet to the exchanger, respectively) with the calculated dewpoint temperature values.

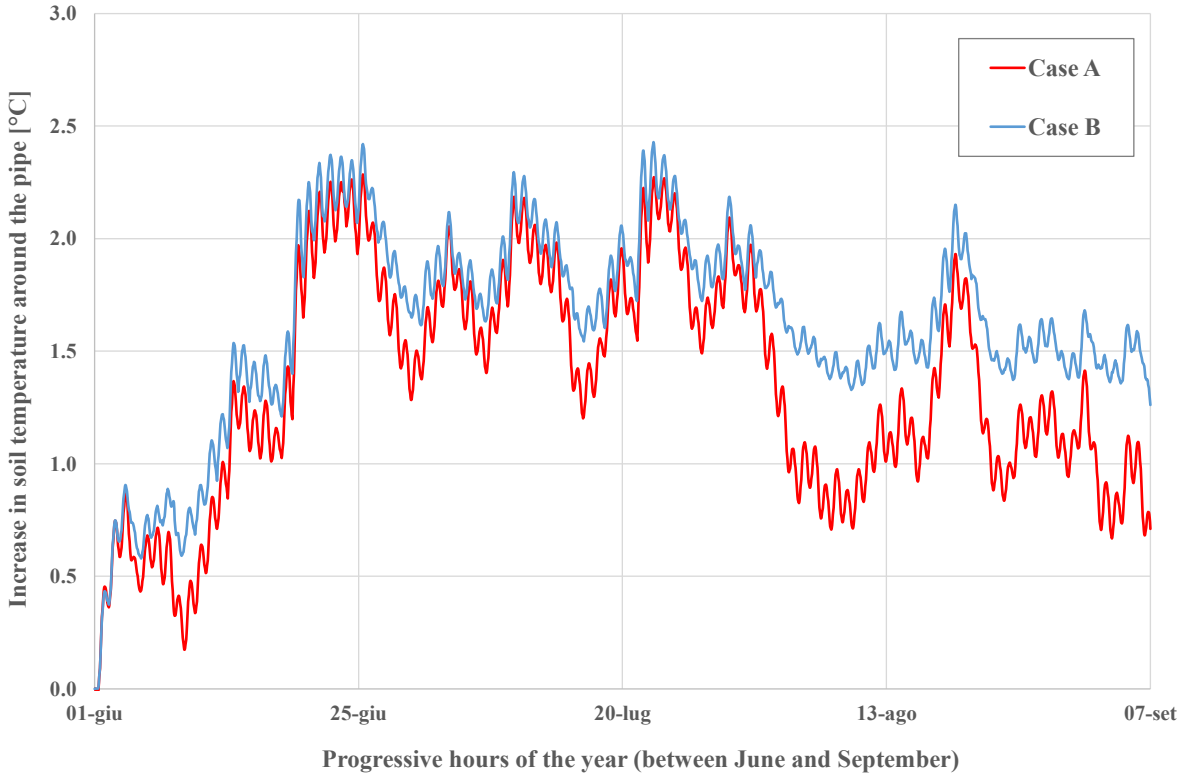

Figure 10. Increase in average soil temperature around the pipe compared to the corresponding undisturbed values of the analysed period (FE simulations).

5. Analysis of Geothermal Model Integrated with Peltier Cells

Peltier cells were applied to the probe described above, considering four different configurations with 1, 3, 5 and 7 cells. Each Peltier cell has a heating power of 0.6 kW

and a cooling power of 0.267 kW. The period analyzed is from 1 June to 1 October of a TMY (Case B)

The aim of the analysis is to evaluate the generation and subsequent collection of condensate water resulting from the vapor-to-liquid phase transition of a defined moist air mixture. This allows for the determination of both the liquid mass flow rate and the corresponding outlet temperature values.

The total dry air mass flow rate is equally distributed between the two branches of the main channel, resulting in a flow rate of 0.0385 kg/s per section. Based on the temperature and relative humidity values, thermodynamic properties are derived, including the humidity ratio, dew point temperature, and specific enthalpy. In particular, by knowing the cooling power of the Peltier cells and the dry air flow rate, the enthalpy reduction due to heat extraction is quantified.

Moreover, the enthalpy of the dry air stream at saturation is evaluated. By comparing this value with enthalpy after the cooling phase, it is possible to determine whether condensation occurs within the system.

As an example, the Psychrometric Chart shows the process obtained on 3 June of a TMY at 2 p.m., considering 1, 3, 5 Peltier cells (Figure 11).

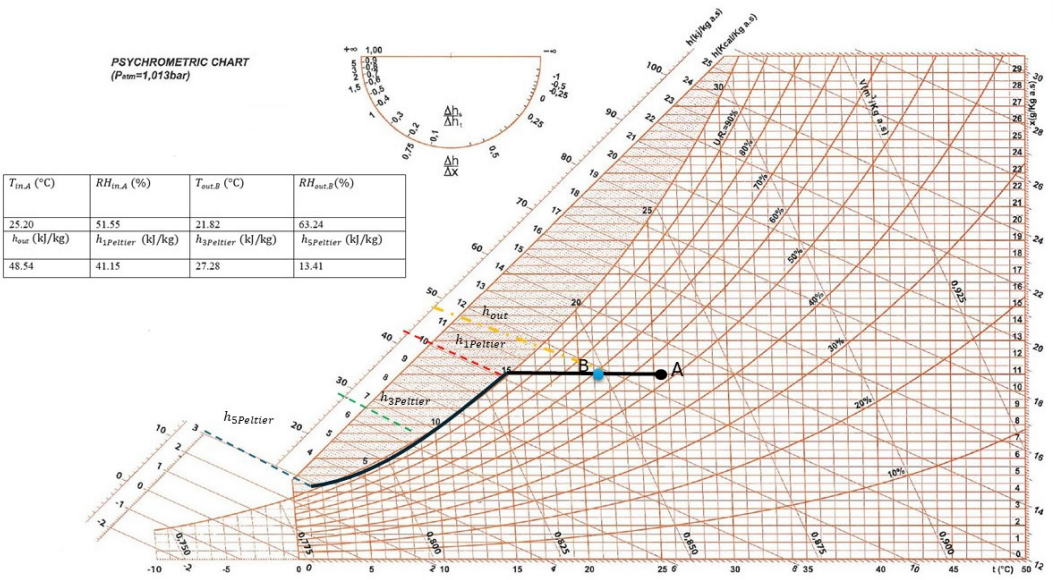

Figure 11. Psychrometric chart of the process, considering 1, 3, and 5 Peltier cells.

The Figure 12 illustrates the evolution of the condensate mass flow rate over time, across the four analyzed case studies.

From 1 June to 1 October of a TMY, the condensed liquid flow rate exhibits a fluctuating trend, marked by multiple peaks throughout the analyzed period. Values range from approximately 0.005 g/s in the initial configuration with 1 Peltier cell to nearly 0.5 g/s in the final setup with 7 Peltier cells. It is important to note that, in the first configuration (1 Peltier cell), due to the specific thermal conditions, condensation does not occur consistently along the pipeline.

During summer operation, passing through the geothermal system can, in some cases, lower the air temperature below the dew point, resulting in the condensation of water vapor. However, it is important to note that the amount of water vapor condensed during this phase is minimal. A significant dehumidifying effect can only be achieved after the air passes through the section equipped with Peltier cells or another active cooling device.

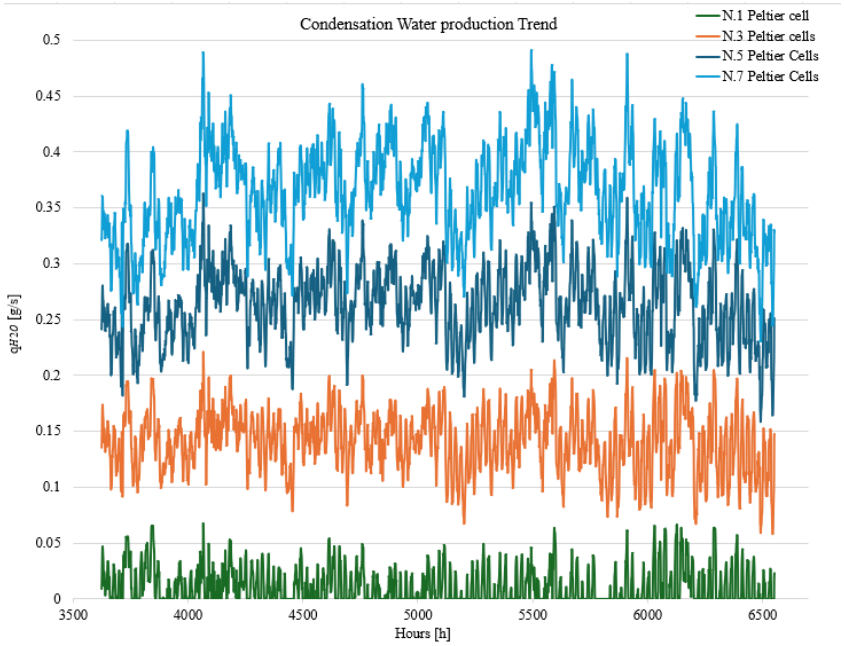

Figure 12. Condensation water production Trend (1 June–1 October of a TMY).

In parallel, the thermal output of the integrated Peltier cell model was evaluated, with its corresponding trend illustrated in Figure 13.

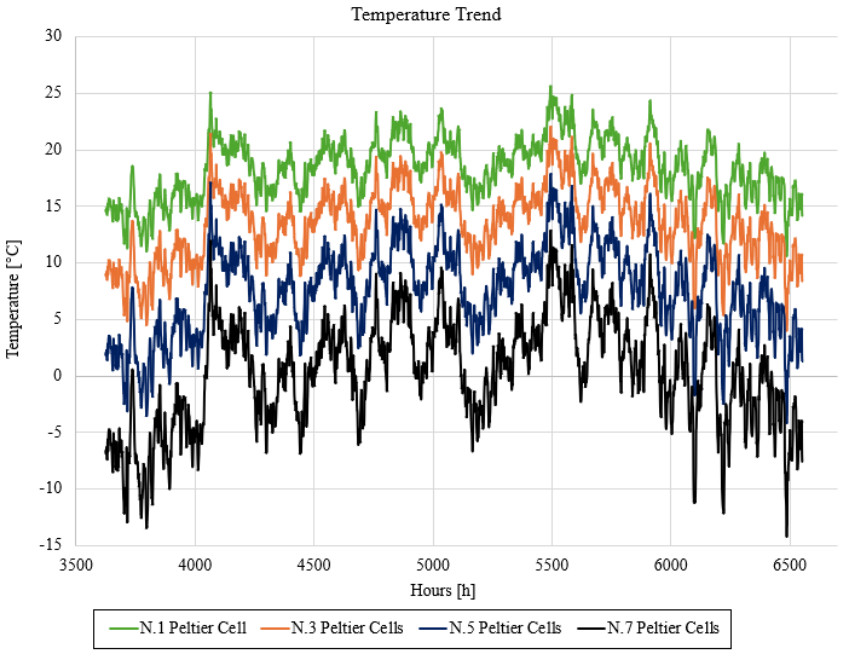

Figure 13. Outlet Temperature Profile After the Peltier Cell Section (1 June–1 October od a TMY).

In the initial configuration with one Peltier cell, outlet temperatures range from approximately 10 °C to 25 °C. As the number of Peltier cells increases, the cooling effect becomes more pronounced, with temperatures approaching 5 °C. In the final configuration (seven Peltier cells), the supplied power reaches levels sufficient to produce sub-zero temperatures. However, this last scenario is included for illustrative purposes only, as temperatures should not drop below a critical threshold to avoid frost formation, which could significantly compromise the integrity and functionality of the device.

6. Conclusions

This paper presents a preliminary analysis aimed at developing a new device that allows for indoor air conditioning and water recovery/storage, reducing energy consumption and combatting water shortages.

The system features a horizontal EAHX integrated with a series of Peltier cells. A fan drives the airflow, which first passes through the EAHX for initial thermal conditioning. The air is then divided into two separate streams that flow across the opposing surfaces of the Peltier cells: one stream passes over the cold side, undergoing sensible and latent cooling with dehumidification, while the other flows over the hot side, resulting in heating.

The analysis presented in this work focuses on the investigation of the thermal conditions of the soil and their influence on the condensation in the horizontal pipe and on the cooling effect. The solution of a Finite Element Method (FEM) was implemented by combining a 3D model, developed in COMSOL Multiphysics®, with a 1D model. The boundary conditions and the thermophysical characteristics of Palermo and TMY of Palermo were used. The results of the first three months (between June and August) show that the exchanger can cool the humid outside air by bringing, on average, its temperature and relative humidity from values of $T_{a,in}$ = 28 °C and RH_{in} = 58% to $T_{a,out}$ = 25.5 °C to RH_{out} = 66.40%. On average, therefore, the EAHXs was able to cool the outside air by about 2.5 °C (keeping, for almost the entire period analyzed, the specific humidity values of the incoming air constant). The average powers exchanged in the three months analyzed for Case A and Case B are equal to 187.89 W and 192.85 W, respectively. Corresponding to these values are values of heat energy subtracted from the air equal to 239.37 kWh and 222.55 kWh, respectively. These preliminary results show that nighttime pre-cooling of the ground (Case A) can lead to a percentage increase in EAHXs efficiency of about 7.56% compared with Case B. Further and more accurate analysis is needed to define possible criteria for optimizing this possible mode of operation.

The system is highly adaptable, with modular components that can be customized or replaced with equivalent parts to suit different contexts. While atmospheric water extraction is typically associated with complex, expensive technologies, this solution is designed to be simple, low-cost, and eco-friendly. Built from locally available materials—like plastic tubing for geothermal pipes and recycled Peltier cells from old electronics—itis ideal for on-site assembly in resource-limited settings.

Its innovation lies in repurposing cooling technologies from electronics and applying them to geothermal systems, enhancing performance with minimal infrastructure. The device can also operate off-grid when paired with solar panels or micro wind turbines, making it especially valuable for remote or underserved areas with limited access to clean water and electricity.

Future developments will focus on optimizing the system by evaluating various scenarios, including different climatic conditions, soil types, system sizes, and the number and spatial configuration of the Peltier cells.

Author Contributions: Conceptualization, C.B. and P.M.C.; methodology, A.B.; software, A.B. and M.S.; validation, A.B., M.S. and M.B.; formal analysis, A.B. and M.S.; investigation, C.B., V.L.B. and M.B.; resources, C.B. and M.B.; data curation, V.L.B.; writing—original draft preparation, M.B.; writing—review and editing, C.B. and V.L.B.; visualization, P.M.C.; supervision, C.B.; project administration, C.B.; funding acquisition, C.B. and M.B. All authors have read and agreed to the published version of the manuscript.

Funding: This study is funded by the "European Commission—Next Generation EU"—PNRR M4—C2–investimento 1.1: Fondo per il Programma Nazionale di Ricerca e Progetti di Rilevante Interesse Nazionale (PRIN)—PRIN 2022PNRR cod. F53D2300971 0001 "AIRcon.WATER (Air conditioning

and Water from Air, by Thermal Earth Recovery)", Università del SALENTO CUP F53D23009710001, Università degli Studi di PALERMO CUP B53D23027020001.

Data Availability Statement: The original contributions presented in this study are included in the article. Further inquiries can be directed to the corresponding author.

Conflicts of Interest: The authors declare no conflicts of interest.

Abbreviations

A	internal cross-sectional area of the pipe [m^2]
B	amplitude of the sinusoid [K]
c_{pa}	specific heat of moist air [$J \cdot kg^{-1} \cdot K^{-1}$]
C_s	volumetric heat capacity of the soil [$J \cdot m^{-3} \cdot K^{-1}$]
d	time expressed in days
d^*	time-lag constant [days]
D	diameter, [m]
h_{conv}	convective heat transfer coefficient [$K \cdot m \cdot W^{-1}$]
$\dot{m}$	mass flow rate [$kg \cdot s^{-1}$]
Nu	Nusselt number
p_v	partial vapor pressure [$N \cdot m^{-2}$]
Pr	Prandtl number
$\dot{q}$	heat flux per unit length [$W \cdot m^{-1}$]
R	equivalent thermal resistance [$K \cdot m \cdot W^{-1}$]
Re	Reynolds number
RH	relative humidity of the air
t	time, [s]
T	temperature [K]
T_0	annual average value of the air temperature [K]
x	horizontal coordinate along the pipe [m]
z	vertical coordinate [m]
Greek letters	
α	thermal diffusivity of soil [$m^2 \cdot s^{-1}$]
γ	dumping constant, [m^{-1}]
λ	thermal conductivity [$W \cdot m^{-1} \cdot K^{-1}$]
ρ	density [$kg \cdot m^{-3}$]
τ	period of the sinusoid, [s]
ω	pulsation [day^{-1}]
ξ	friction factor
Subscripts	
a	air
as	air-to-soil
ap	air-to-pipe
dp	dew point
i	inner
in	inlet
inf	inferior
o	outer
out	outlet
p	pipe
ps	pipe-to-soil

Acronyms

BHE	Borehole Heat Exchanger
EAHXs	Earth-to-Air Heat eXchanger system
FE	Finite Element
PDE	Partial Differential Equation
PE	cross-linked polyethylene
TMY	Typical Metereological Year
TRT	Thermal Response Test

References

1. Gondal, I.A.; Masood, S.A.; Amjad, M. Review of geothermal energy development efforts in Pakistan and way forward. *Renew. Sustain. Energy Rev.* **2017**, *71*, 687–696. [CrossRef]
2. Khan, A.; Bradshaw, C.R. Quantitative comparison of the performance of vapor compression cycles with compressor vapor or liquid injection. *Int. J. Refrig.* **2023**, *154*, 386–394. [CrossRef]
3. Ghosal, M.K.; Tiwari, G.N. Modeling and parametric studies for thermal performance of an earth to air heat exchanger integrated with a greenhouse. *Energy Convers. Manag.* **2006**, *47*, 1779–1798. [CrossRef]
4. Congedo, P.M.; Baglivo, C.; Bonuso, S.; D'Agostino, D. Numerical and experimental analysis of the energy performance of an air-source heat pump (ASHP) coupled with a horizontal earth-to-air heat exchanger (EAHX) in different climates. *Geothermics* **2020**, *87*, 101845. [CrossRef]
5. Vaz, J.; Sattler, M.A.; Brum, R.S.; dos Santos, E.D.; Isoldi, L.A. An experimental study on the use of Earth-Air Heat Exchangers (EAHE). *Energy Build.* **2014**, *72*, 122–131. [CrossRef]
6. Cao, S.; Li, F.; Li, X.; Yang, B. Feasibility analysis of Earth-Air Heat Exchanger (EAHE) in a sports and culture center in Tianjin, China. Case Stud. *Therm. Eng.* **2021**, *26*, 101054. [CrossRef]
7. Yang, J.; Song, W.; Zhang, H.; Wang, J.; Dong, J. Experimental study on the characteristics of radiation floor cooling system based on an earth–air heat exchanger. *Energy Build.* **2023**, *296*, 113338. [CrossRef]
8. Bonuso, S.; Panico, S.; Baglivo, C.; Mazzeo, D.; Matera, N.; Congedo, P.M.; Oliveti, G. Dynamic Analysis of the Natural and Mechanical Ventilation of a Solar Greenhouse by Coupling Controlled Mechanical Ventilation (CMV) with an Earth-to-Air Heat Exchanger (EAHX). *Energies* **2020**, *13*, 3676. [CrossRef]
9. Salhein, K.; Kobus, C.J.; Zohdy, M.; Annekaa, A.M.; Alhawsawi, E.Y.; Salheen, S.A. Heat Transfer Performance Factors in a Vertical Ground Heat Exchanger for a Geothermal Heat Pump System. *Energies* **2024**, *17*, 5003. [CrossRef]
10. Luo, M.; Gan, G. Numerical investigation into the thermal interference of slinky ground heat exchangers. *Appl. Therm. Eng.* **2024**, *248*, 123215. [CrossRef]
11. Baglivo, C.; Bonuso, S.; Congedo, P.M. Performance Analysis of Air Cooled Heat Pump Coupled with Horizontal Air Ground Heat Exchanger in the Mediterranean Climate. *Energies* **2018**, *11*, 2704. [CrossRef]
12. Sehli, A.; Hasni, A.; Tamali, M. The Potential of Earth-air Heat Exchangers for Low Energy Cooling of Buildings in South Algeria. *Energy Procedia* **2012**, *18*, 496–506. [CrossRef]
13. Al-Ajmi, F.; Loveday, D.L.; Hanby, V.I. The cooling potential of earth–air heat exchangers for domestic buildings in a desert climate. *Build. Environ.* **2006**, *41*, 235–244. [CrossRef]
14. Hollmuller, P.; Lachal, B. Cooling and preheating with buried pipe systems: Monitoring, simulation and economic aspects. *Energy Build.* **2001**, *33*, 509–518. [CrossRef]
15. Zhang, D.; Zhang, J.; Liu, C.; Yan, C.; Ji, J.; An, Z. Performance measurement and configuration optimization based on or-thogonal simulation method of earth-to-air heat exchange system in cold-arid climate. *Energy Build.* **2024**, *308*, 114001. [CrossRef]
16. Zhou, K.; Mao, J.; Li, Y.; Zhang, H. Performance assessment and techno-economic optimization of ground source heat pump for residential heating and cooling: A case study of Nanjing, China. *Sustain. Energy Technol. Assess.* **2020**, *40*, 100782. [CrossRef]
17. Zhao, Y.; Li, R.; Ji, C.; Huan, C.; Zhang, B.; Liu, L. Parametric study and design of an earth-air heat exchanger using model experiment for memorial heating and cooling. *Appl. Therm. Eng.* **2019**, *148*, 838–845. [CrossRef]
18. Niu, F.; Yu, Y.; Yu, D.; Li, H. Heat and mass transfer performance analysis and cooling capacity prediction of earth to air heat exchanger. *Appl. Energy* **2015**, *137*, 211–221. [CrossRef]
19. Kumar Agrawal, K.; Misra, R.; Das Agrawal, G. To study the effect of different parameters on the thermal performance of ground-air heat exchanger system: In situ measurement. *Renew. Energy* **2020**, *146*, 2070–2083. [CrossRef]
20. Sakhri, N.; Menni, Y.; Ameur, H. Effect of the pipe material and burying depth on the thermal efficiency of earth-to-air heat exchangers. *Case Stud. Chem. Environ. Eng.* **2020**, *2*, 100013. [CrossRef]
21. Alqawasmeh, Q.I.; Narsilio, G.A.; Makasis, N. Impact of geometrical misplacement of heat exchanger pipe parallel configuration in energy piles. *Energies* **2024**, *17*, 2580. [CrossRef]

22. Zhou, Y.; Bidarmaghz, A.; Makasis, N.; Narsilio, G. Ground-source heat pump systems: The effects of variable trench separations and pipe configurations in horizontal ground heat exchangers. *Energies* **2021**, *14*, 3919. [CrossRef]
23. Cherif Lekhal, M.; Belarbi, R.; Mokhtari, A.M.; Benzaama, M.-H.; Bennacer, R. Thermal performance of a residential house equipped with a combined system: A direct solar floor and an earth–air heat exchanger. *Sustain. Cities Soc.* **2018**, *40*, 534–545. [CrossRef]
24. Ghiasi, M.; Wang, Z.; Mehrandezh, M.; Paranjape, R. Enhancing efficiency through integration of geothermal and photovoltaic in heating systems of a greenhouse for sustainable agriculture. *Sustain. Cities Soc.* **2025**, *118*, 106040. [CrossRef]
25. Jathunge, C.B.; Dworkin, S.B.; Wemhöner, C.; Mwesigye, A. Performance investigation of a solar-assisted ground source heat pump system coupled with novel offset pipe energy piles and solar PVT collectors for cold climate applications. *Appl. Therm. Eng.* **2025**, *265*, 125568. [CrossRef]
26. Shahsavar, A.; Azimi, N. Performance evaluation and multi-objective optimization of a hybrid earth-air heat exchanger and building-integrated photovoltaic/thermal system with phase change material and exhaust air heat recovery. *J. Build. Eng.* **2024**, *90*, 109531. [CrossRef]
27. Bhutta, M.M.A.; Hayat, N.; Bashir, H.M.; Khan, A.R.; Ahmad, K.N.; Khan, S. CFD applications in various heat exchangers design: A review. *Appl. Therm. Eng.* **2012**, *32*, 1–12. [CrossRef]
28. Congedo, P.M.; Lorusso, C.; Baglivo, C.; Milanese, M.; Raimondo, L. Experimental validation of horizontal air-ground heat exchangers (HAGHE) for ventilation systems. *Geothermics* **2019**, *80*, 78–85. [CrossRef]
29. Li, C.; Jiang, C.; Guan, Y.; Chen, K.; Wu, J.; Xu, J.; Wang, J. Simplified method and numerical simulation analysis of pipe-group long-term heat transfer in deep-ground heat exchangers. *Energy* **2024**, *299*, 131533. [CrossRef]
30. Buscemi, A.; Beccali, M.; Guarino, S.; Lo Brano, V. Coupling a road solar thermal collector and borehole thermal energy storage for building heating: First experimental and numerical results. *Energy Convers. Manag.* **2024**, *291*, 117279. [CrossRef]
31. Incropera, F.P.; DeWitt, D.P.; Bergman, T.L.; Lavine, A.S. *Fundamentals of Heat and Mass Transfer 5th Edition with IHT2.0/FEHT with Users Guides*; Wiley: Hoboken, NJ, USA, 2001.
32. Gnielinski, V. On heat transfer in tubes. *Int. J. Heat Mass Transf.* **2013**, *63*, 134–140. [CrossRef]
33. Tsilingiris, P.T. Thermophysical and transport properties of humid air at temperature range between 0 and 100 °C. *Energy Convers. Manag.* **2008**, *49*, 1098–1110. [CrossRef]
34. Gatley, D.P. *Understanding Psychrometrics*, 3rd ed.; The American Society of Heating, Refrigerating and Air-Conditioning Engineers, Inc.: Atlanta, GA, USA, 2013.
35. Congedo, P.M.; Baglivo, C.; Negro, G. A New Device Hypothesis for Water Extraction from Air and Basic Air Condition System in Developing Countries. *Energies* **2021**, *14*, 4507. [CrossRef]